Automatic defects detection using neighborhood windows features in tire X-ray images

Yousef Sedaghat[a], Naser Parhizgar[a,*], Ahmad Keshavarz[b]

[a]Department of Electrical Engineering, Shiraz Branch, Islamic Azad University, Shiraz, Iran
[b]IoT and Signal Processing Research Group, ICT Research Institute, Faculty of Intelligent Systems Engineering and Data Science, Persian Gulf University, 7516913817 Bushehr, Iran

(Communicated by Ehsan Kozegar)

Abstract

Ensuring the production of non-defect high-quality tires is an essential part of the tire industry. X-ray inspection is one of the best methods to detect tire defects. In this paper, a new approach has been presented for detecting tire defects in X-ray images based on an entropy filter, the extraction of texture properties of patches by Local Binary Pattern, and, finally, the classification of defects using the Support Vector Machine method. In the proposed method, an entropy filter was first applied to the input. The parts of the image with different patterns were then selected as candidate regions and these regions were classified by the patch classifier. All the defects were detected and classified and, finally, the efficiency of the algorithm was evaluated. By applying this algorithm to the dataset the best performance was obtained by the LBP descriptor and the linear SVM classifier with 98% defect location accuracy and 97% defect detection accuracy were achieved. In order to analyze the performance, used the deep model as a classifier, thus demonstrating that the deep model has a high capability for learning complex patterns. This proposed method is sensitive to local texture and could well describe texture information, which is appropriate for most kinds of tire defects.

Keywords: Tire Defects Detection, Local Binary Pattern, Entropy Filter, Patch Classification, Support Vector Machine
2020 MSC: 94A17, 28D20

*Corresponding author
Email addresses: m_y_sedaghat@yahoo.com (Yousef Sedaghat), n.parhizgar@gmail.com (Naser Parhizgar), a.keshavarz@pgu.ac.ir (Ahmad Keshavarz)

1. Introduction

Nowadays, defect detection is one of the most important issues in final inspections and quality controls in industry. Research has shown that the quality of tires is linked to the safety and health of humans [7]. On the other hand, automation of the defect detection process is one of the most important and challenging problems in industrial inspection. Currently, in most tire manufacturing companies, identifying the defects and separating defective products are often done by operators, which, in addition to requiring more manpower and time, may not have a good return as well. Therefore, automatic tire defect detection and classification will bring reasonable results. The purpose of this research is to improve the system of supervision and inspection of the production line and increase the quality of the manufactured tires. In general, there are two types of product quality inspections: destructive and nondestructive tests. Nondestructive techniques are used to test the surface or internal defects without destroying, or interfering with, the internal components. The usual methods used in nondestructive tests are: acoustic emission, magnetic particles, eddy current, ultrasonic test, and radiography test [38]. The total effects available for these techniques are very limited and in some cases are only suitable for a particular defect type. For example, the liquid penetrant and magnetic particles tests are used to find surface defects. The Eddy current test is used only in cases where the part is not magnetized. Although the ultrasonic test can detect a wide range of defects, the interpretation of the output signal is difficult and has little documentation capability. Radiographic imaging is one of the most widely used methods for detecting internal defects as well as finding changes in the composition, thickness measurement, and determining the location of extra or defective parts that are normally hidden from human sight. This method, especially the X-ray imaging, is the most effective tool for inspecting and monitoring the products, especially in tire inspection [9]. Therefore, in this paper, an approach based on image analysis and learning methods is presented for detecting and evaluating heterogeneous regions of defects in Xray images. It should be noted that this strategy, in addition to identifying all types of defects, classifies them that can be applied to an automation process as inline in tire manufacturing companies.

2. Literature review

Researchers have been using image processing and pattern recognition techniques to make automatic inspection as desirable and highly reliable as possible. Non-destructive inspection technology has been widely used in various fields including steel [28], casting and welding [8, 17], textiles and fabric [3], TFT-LCD panels [24], Nano-structures [36, 37], aluminum surfaces with titanium coating [33] and semiconductors [1]. Defect equation detection technology based on radiographic images is also used to diagnose weld, fabric and tire defects. We can say that machine vision-based methods can be divided into three categories: Shearography imagebased methods [40], X-ray radiography image-based methods [27], and optical image-based methods of the CCD camera [2]. In general, most of the methods have been conducted to automatically detect surface defects [2, 14, 15, 17, 23, 32, 39]. On the other hand, there are major problems in the automatic detection of tire defects, which are due to the characteristics of their radiographic images. These problems are [39]:

1. The intensity of brightness in these images change abruptly because the tires have complex multilayer structures, consisting of layers with different textures and thicknesses. Different tires or different layers of the same tires vary in terms of structure, thickness, and raw materials, which help to vary the intensity in different parts of the radiographic image.
2. Different defects occur in forms, shapes, intensities, and scales. Instances of such defects are the existence of foreign objects, bubbles, cords distances, belts splices (open joints or overlaps),

free extra cords, cords bulks and cords bendings in tires. Applying only one feature space for recognition of all these disadvantages is not suitable.

Research has shown that compared with other machine vision applications, research on defect detection of tires is still very limited and more studies are needed to achieve highly desirable results [12]. In [11], a method for tire detection has been presented using laser shearography, which is a combination of an improved image based on Curvelet and Canny operators. However, there are limitations to this method; For example it does not work for the detection of a non-metallic foreign object such as a plastic object. In [27], a method for foreign object and bubble detection in X-ray radiography images has been presented, which is based on the general variance of image and edge detection. However, in this method the contours of detected defects are incorrect and incomplete, so that the complete extraction of defects is difficult. In [26], Prabha PA et al. multi scale saliency defect detecting algorithms is implemented to obtain the boundaries and range of defect in industrial products. Li [16] investigated the detection of tires with X-ray radiography images and fuzzy edge detection methods. Chien CH et al. [4] presented a deep convolutional sparse-coding network is built for tire defect classification for extraction of features. In [35], a defect detection algorithm based on the representation of all data has been proposed, in which the difference in the distribution of these representation coefficients has been used as an indicator for detecting a defective region. Compared with the method of automatic range selection for wavelet reconstruction method in [30], it shows good results. However, defect detection using brightness variation has been a nearly trouble-free method. Zhu [41] presented a method for defect detection of bubbles in tires using digital holography. The methods based on ground truth or templates evaluate the difference between these images and their templates for defect detection [18]. It is worth noting that the automated inspection and the diagnostic processes of defects such as fabric, casting steel, welding, etc. have the same goals and are very similar to the process of defect detection in tires. In [21], a convenient decomposition method for inspecting patterned texture has been described. Defect detection methods for motif-based patterned textures include Fourier transform [31], Wavelet transform [10], Gabor filters [19], Template Matching [6], Co-occurrence Matrix [13], and a method for patterned two-dimensional texture images [22]. From among these methods, the Wavelet transform method has been the most efficient. The wavelet-based binary image method was developed by Li [17], which could prove to be very effective in detecting defects in casting. This detection has been done using local variations in the intensity of the image. However, it is still difficult to extract the characteristics of tire radiographic images due to its multi-layered and multi-textural properties. In [5], a supervised feature embedded deep learning based tire defects classification method using deep image features proposed and composed images belonging to six typical defect categories. A new algorithm of detecting joints in the belt is proposed in [34] and the defect is determined by calculating the difference between the block containing the joint and its corresponding standard blocks but it is not applicable to aperiodic tires. In this paper, a real-time method has been proposed based on image analysis using entropy filters and classification of candidate regions using local descriptions. The algorithm presented in this paper detects and classifies defects of X-ray images and refers to one of the eight classified defects shown in Fig. 2. The method is well-suited to X-ray tire images and can be extended to other issues. In the next section, the proposed strategy will be described completely.

3. Dataset

To carry out this research, field visits have severally been done in some tire manufacturing companies including the production line inspection of Dena Tire and Rubber Manufacturing Company in Iran. In general, the structure of each tire consists of two main regions named the 'Belt' region

(middle region) and the 'Shoulder' region (the two lateral regions). The defects addressed in this research are not normally visible by human sight but are shown by tire X-ray imaging. These defects occur mainly in the belt and shoulder regions. The presented algorithm, detects all eight defects of tire images and classifies them. In case no defect is detected, then the tire is labeled as normal (non-defect) type. Therefore, an image can have one of the nine different labels. In this regard, 1040 original defective and non-defective X-ray images containing nine typical defect categories and normal category, collected were divided into two categories of training and test in order to construct the dataset for evaluating the accuracy rate of the system in this paper. In this segmentation, the images were equally divided to 520 training images and 520 test images; samples of these images, namely, Belt Foreign Body (BFB), Shoulder Foreign Body (SFB), Shoulder Bubble (SB), Cords Distance (CD), Belts Splice (BS), Shoulder Free Cord (SFC), Shoulder Bulk Cords (SBC), Shoulder Cords Bending (SCB) as shown in Fig. 2 (a to g) respectively.

4. The proposed method

The purpose of this paper is to provide a strategy for solving the challenges available in this region in order to improve the effectiveness of this strategy. In this line, a method for describing a tire image in two different modes is presented first. The proposed strategy is robust against images with different brightness rates and noise. Subsequently, Local Binary Pattern (LBP) information is extracted from these regions by spatially segmenting the image. Each of these regions is classified into two classes of defected and non-defected and then based on this classification, the corresponding heat-map image is generated. Finally, defective regions are detected on the heat-map images by morphology operations and their type is detected. It should be noted that the proposed strategy is resistant to images with different brightness, and various patterns, and has high efficiency and speed. The following section describes the system training and the system processing phases.

4.1. System Training Phase

The training phase in this paper initially tries to divide the images into a series of overlapping regions of size $n*n$ called 'patch'. Then local descriptions are extracted for each of these patches and the classifier is learned. The block diagram in Fig. 1 illustrates the process of learning the patches of the training images. According to this strategy for learning defective and normal patches, the input image is first normalized and then divided into a series of overlapping regions with a constant size. In the following, normal and defective patches are extracted by extracting the LBP description.
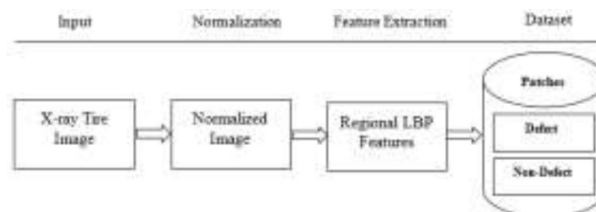

Figure 1: Process of learning patches of the training images

4.1.1. Normalizing the Images

As discussed earlier, tire images can have variable brightness levels, which cause different regions of the image to have different patterns. Histogram equalization is used to reduce this effect in the first stage of processing. In this process, it is used to convert the values of image pixels to new values

a- The presence of an foreign body in shoulder region
- **Belt Foreign Body (BFB)**

b- The presence of an foreign body in belt region
- **Shoulder Foreign Body (SFB)**

c- The presence of bubble in the shoulder region
- **Shoulder Bubble (SB)**

d- The presence of distance between the cords in Shoulder region
- **Cords Distance (CD)**

e- Splice between belts layers in the belt region
- **Belt splice (BS): Open joint / Overlap**

f- The presence of free extra cord in the shoulder region
- **Shoulder Free Cord (SFC)**

g- Overlapping of cords in shoulder region
- **Shoulder Bulk Cords (SBC)**

h- Bending of the cords in the shoulder region
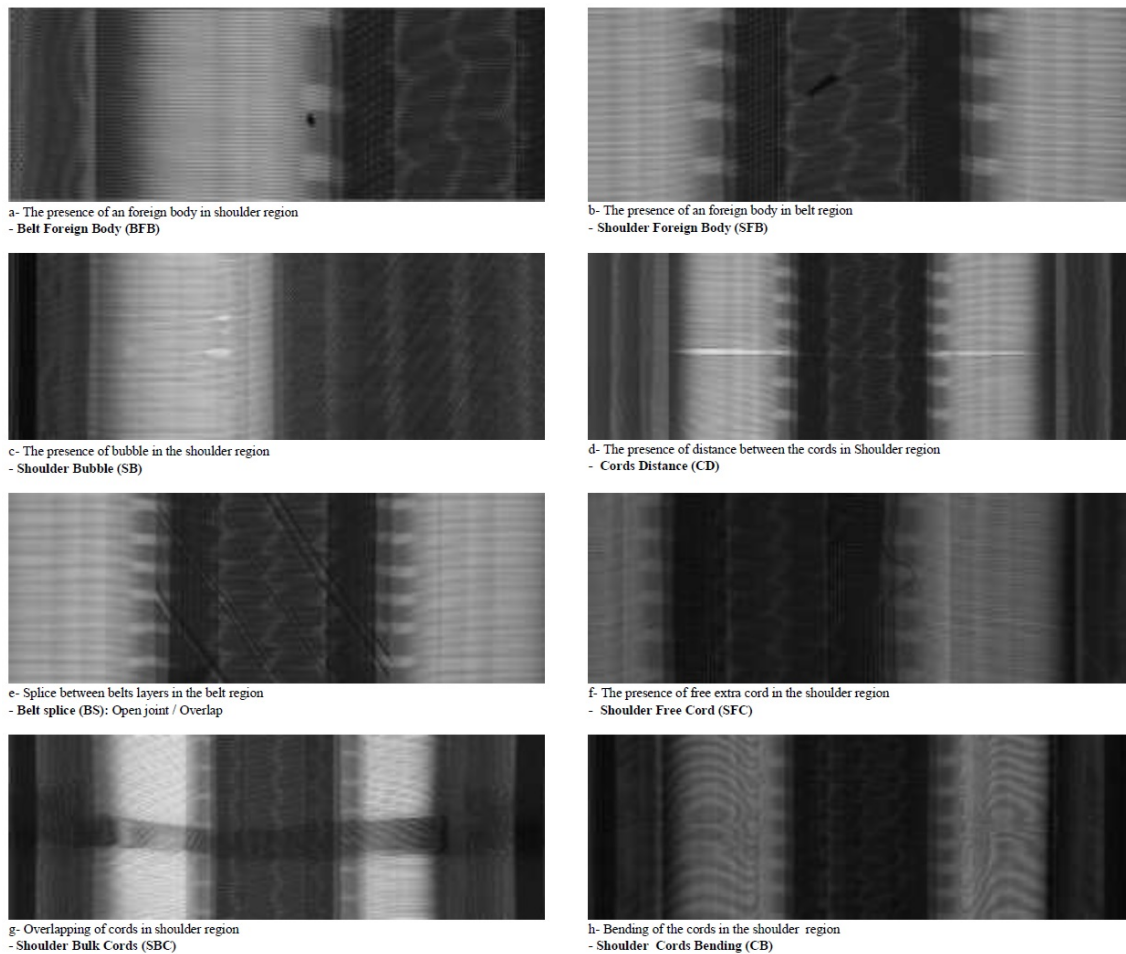- **Shoulder Cords Bending (CB)**

Figure 2: Tire defects types in X-ray images

in such a way that the histogram of the image is uniform in order to increase the image contrast. An equalized histogram is defined by equation (4.1):

$$g_{i,j} = (L-1) \sum_{n=0}^{I_{i,j}} p_n \qquad (4.1)$$

In the above equation, $g_{i,j}$ is the normalized image and $I_{i,j}$ represents the input image. L represents the number of brightness levels for the image, usually 256, and p_n is the normalized histogram of the input image defined by equation (4.2):

$$p_n = \frac{\text{number of pixels with intensity n}}{\text{total number of pixels}}, \qquad n = 0, 1, ..., L-1 \qquad (4.2)$$

4.1.2. Production of Image Patches

Here is a description of the patch production process. In the process of recognizing tire defects in X-ray images, different regions of the image can generally be classified into two classes: defective and non-defective. We use a banding box on X-ray images to extract the patches. In this paper, about 2000 cropped images have been extracted from different regions of the training regions as 'defective' regions. All of these extracted images were normalized to 10×10 sizes. Then each of the images with the probability of 1/2, was randomly rotated three times in the range of 0 to 300 degrees to produce

3 new image types [29]. The extracted images were folded vertically, horizontally and normally. As a result, three new images were produced. These patches were also given scales 75%, 100%, and 125% to produce three different image types for each patch in the final stage.

Hence, for each defective patch, $3 \times 3 \times 3 \times 0.5 = 13.5$ times were produced which show different versions of a defect. Also, in some defective images, the process of adding low noise was randomly selected with the probability of 1/10. Approximately 27000 patches were generated for the defective class with $13.5 \times 2000 = 27000$.
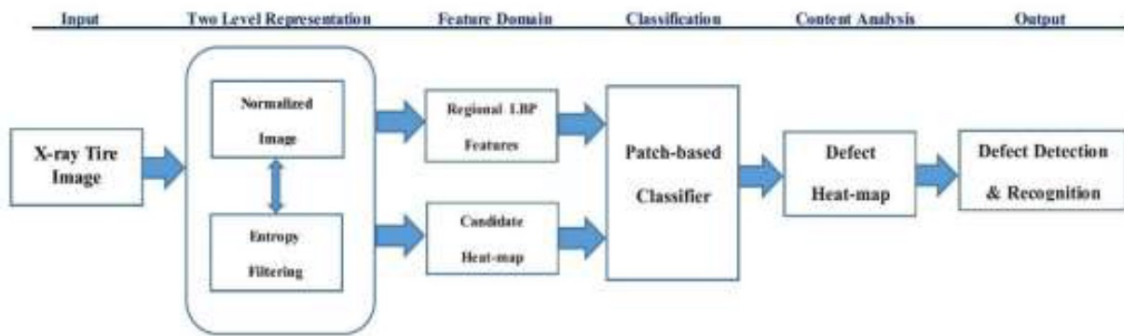

Figure 3: Block diagram of the proposed method

About 25000 patches were randomly extracted from different regions of normal images to produce the patches for non-defective classes and then all of these images were normalized to 10×10 dimensions. Block diagram of the proposed method for the detection of defects in tire images has been shown in Fig. 3. In the proposed method, the input image is described at two different levels. In the first level, the image is normalized to reduce the effect of light conditions on the algorithm. In the second level, the entropy filter is applied to the image to produce a new image which shows highlighted heterogeneity in patterns.

4.2. Data Processing Phase

In the following, the correlation of image regions are compared with a normal reference image using the entropy filter. The regions with low correlation value are selected as candidate regions.

Subsequently, the LBP description is extracted from the normalized image with the help of the generated candidate regions. These regions are classified using the patch classifier to generate the heat map image. The defect location and its types are detected by applying morphological operations and evaluating the regions available in the heat map image. In the next section, these steps have been explained in sequence.

4.2.1. Entropy Filter

Entropy is a criterion for measuring the random rate of a signal. In this paper, we intend to evaluate the image texture by using the entropy filter on the tire image. The entropy filter is defined by equation (4.3):

$$e = -\sum_{i=0}^{L-1} p_i \log_2 p_i \tag{4.3}$$

In this equation, p_i is the probability distribution function (PDF) of brightness in a neighborhood window of a pixel and L indicates the number of brightness levels in that window. A textured image is generated by applying relation (4.3) on the image. In this textured image, the amount of each

pixel is obtained from the entropy of its neighboring pixels according to Eq. (4.2). An example of applying Eq. (4.3) to a tire image with a bubble defect has been shown in Fig. 4. An important parameter that influences the production process of the textured image is the choice of window size in the entropy filter. The size of this window should be chosen in such a way that is smaller than the size of the defect, such that the presence of the defect does change the entropy information of the region. Also, the size of the window should be larger than the size of texture points caused in the image to avoid the entropy changes made by these points themselves. Fortunately, this is not problematic in tire images because the size of the defects in tire images is larger than the size of the texture points. The image obtained from the entropy filter is first divided into overlapping blocks in order to determine the candidate regions. Then in terms of the degree of similarity, each of these blocks is compared with their respective block in the entropy image of the normal tire. If the level of similarity of these blocks is greater than the threshold, then they will be announced as a 'candidate'. As a result, the image regions that may be defective in this section are identified and then generate I_c that represents a candidate image. It should be noted that feature extraction and classification does not run on the entire image. Rather, it is done only in candidate regions.

4.2.2. Regional Local Binary Pattern

Local binary pattern (LBP) is a method of extracting texture information in images [25, 29]. This method is used due to high speed and resolution in many computer vision applications. The normalized image is first divided into overlapping blocks in order to extract features of LPB, then for each block with centered (x_c, y_c) pixel, the LBP descriptor is extracted using Eq. (4.4).

$$LBP_{P.R}(x_c, y_c) = \sum_{k=0}^{P-1} S(I_{(x_k,y_k)} - I_{(x_c,y_c)})2^k \tag{4.4}$$

In Eq. (4.4), $I_{(x_c,y_c)}$ and $I_{(x_k,y_k)}$ represent the gray level of the center pixel and the neighboring pixels located on the circular boundary, respectively. P is the number of neighboring pixels and R represents the radius of the circle. Function S is expressed using Eq. (4.5):

$$S(x) = \begin{cases} 1 \ if \ x \geq 0 \\ 0 \ if \ x < 0 \end{cases} \tag{4.5}$$

After calculating the local binary pattern values for all pixels, the image is divided to several cells and the histogram of each cell is expressed as its local binary pattern description.
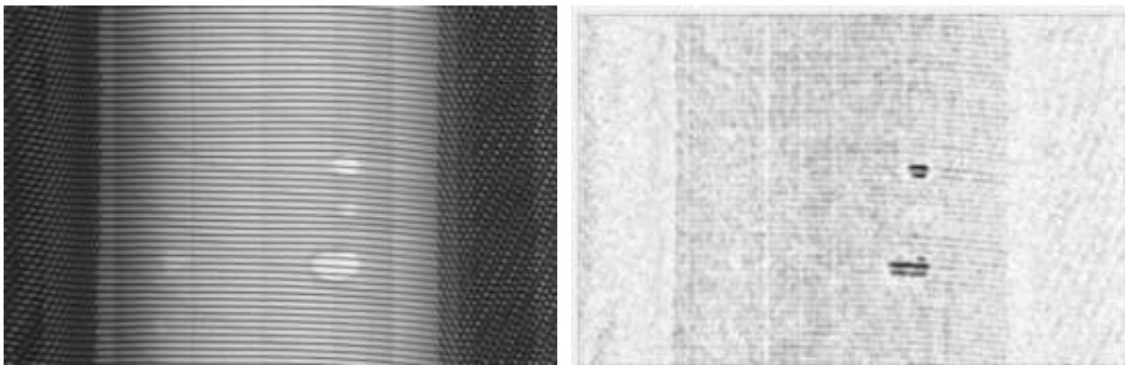

Figure 4: The image obtained from applying the entropy filter on the defective image of bubble

4.2.3. Creation of Heat-Map Image Using the Patch-Based Classifier

In this section, first, the areas that need to be processed in the normalized image are specified using the candidate image. The LBP description of these areas is then classified into one of two normal and defective classifications, using the SVM model [20]. If a patch is assigned to a classification with defect, then, according to Algorithm 1, a Gaussian model with the center of that patch is added to the heat-map image.

It should be noted that the size of the heat-map image is considered equal to the input image and the initial values of each pixel is zero.

In algorithm 1, N_r shows the number of rows, N_c is the number of columns in normalized image and C_d represents the class of defects. Fig. 5 shows an example of a generated heat-map image for defect of splice between the belt layers in the tire in which defective areas are clearly identified.

Algorithm 1: Heatmap Generation
___
1 : Input $= g, I_c$
2 : Output $= I_{\text{Heatmap}}$
3 : For $j = 1$ to N_r
4 :   For $k = 1$ to N_c
5 :   If $I_c(i, j)_w = $ Candid
6 :   If $SVM(LBP(I_N(i, j)_w))$ is in C_d do
7 : $I_{\text{Heatmap}}(i, j)_w = G(w) + I_{\text{Heatmap}}(i, j)_w$
8 :   End if
9 :   End if
10 :   End for
11 : End for
___

4.2.4. Final Detection of Location and Type of Defects

In this section, using the image of heat-map, the location of defect and its type are detected. First, by using morphological operations, the objects smaller than the first threshold value and larger than the second threshold value are eliminated as noise. The remaining objects in the image define the defect's location. Considering the fact that in this paper eight types of defects are discussed in Fig. 2, the classification is done using the previous information about the types of defects. We use these defects' information to classify the detected region into one of the eight defect types.

Generally, these defects are distinguished using the following kinds of information: the location of the defect is used to specify the belt or shoulder regions, and the brightness level of the detected region is used to distinguish the bubble defects and foreign objects. The number and amount of dispersion of the recognized regions and also the defects' structures are used to classify the defects. It should be noted that conditional conditions are used for this information.

5. Results

In this section, the results obtained from applying the proposed strategy on the dataset are examined as shown in Fig. 6. The results section consists of three parts. In the first part, the efficiency of the suggested strategy to the detection of defects in tires is investigated. In the second part, the accuracy rate of the algorithm in the classification of the defect type is discussed. In the third part, the effect of problem parameters, data augmentation, and runtime of the algorithm are investigated.
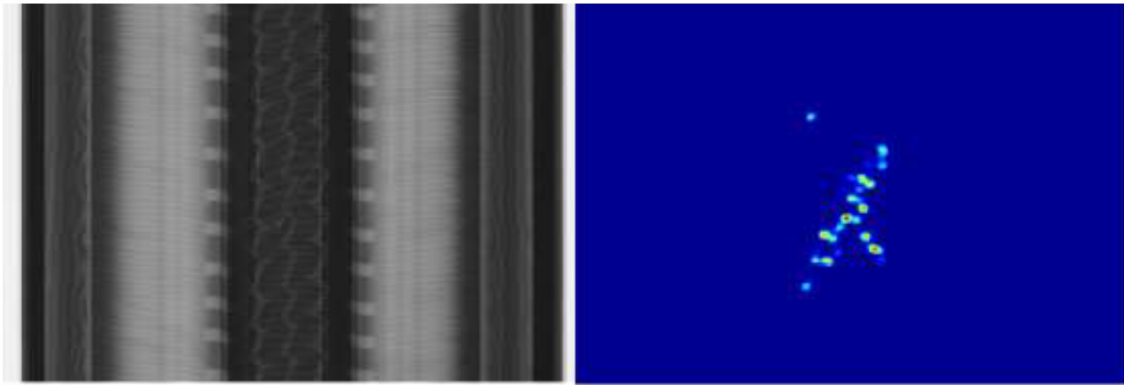
Figure 5: A sample of the heat-map of a defective image

5.1. Efficiency of the Algorithm in Detecting Defective Areas

In this section, the results obtained from the application of the proposed algorithm will be evaluated to identify defective regions in X-ray images.

As previously stated, there are eight different types of tire defects in the dataset used in this study. An example of these defects, along with the explanations, is given in Fig. 2. The main objective in defining defective regions is to provide an algorithm that extracts all regions of defect and classifies the remaining regions as normal regions. Therefore, Precision, Recall and Accuracy criteria are used to analyze and investigate the system efficiency. The precision criterion shows the number of data that is detected correctly relative to the total detected data. In other words, this criterion measures the number of pieces of data which have been identified as 'defective' and are actually in the classification of defective data.

The Recall criterion shows the proportion of detected data to the total available data. In other words, this criterion measures the number of detected defective regions in relation to the total number of defective regions. The Accuracy criterion is the ratio of the data that are detected correctly to the total available data. These criteria are defined by the following equations as defined in Eq. (5.1) to (5.3):

$$Re = \frac{TP}{TP + FN} \tag{5.1}$$

$$Pr = \frac{TP}{TP + FP} \tag{5.2}$$

$$Acc = 100 \times \frac{TP + TN}{P + N} \tag{5.3}$$

where:

- **True Positive**: The number of defects that are properly classified.

- **True Negative**: The number of non-destructive defects that are properly classified.

- **False Positive**: The number of non-destructive defects that are classified incorrectly.

If $Pr = Re = Acc$, then it means that all defects have been correctly detected and no errors have occurred, and that this mode is ideal. Table 1 shows the obtained results. We have used five different classifiers in order to better analyze the results.

These classifiers include the KNN classification with a neighborhood value of 3 and 5, the random forest classification, and the SVM classification with two linear and RBF kernels. It should be noted that the description of LBP as the final attribute has been used.

In Table 1, the obtained accuracy value has been sorted ascendingly in which the highest accuracy value refers to the linear SVM classifier. Also, the least amount of obtained accuracy value is for the KNN classifier with 3 neighborhoods. This case shows that neighborhood 5 is more resistant to noise than neighborhood 3, and has a high accuracy rate. It should be noted that more neighborhoods were used for this case, but it reduced the accuracy. In Table 1, due to the fact that the size of the input images is 600×600, and the size of the patches is 10×10, the number of generated patches for each image is about 3000. On average, for each test image some 100 patches out of 3000 patches are related to the classification of defective ones and the others are normal.

Ideally, for the results in Table 1, for each image there are 2900 normal and 100 defective patches. According to the efficiency rate of the various classifiers, the highest efficiency has been achieved by the SVM-linear classifier. Another method for measuring the efficiency of automatic defect detection methods is to calculate the detection rate as defined in Eq. (5.4):

$$\text{Detection Rate} = 100 \times \left(\frac{N_{cc} + N_{dd}}{N_{\text{total}}} \right) \tag{5.4}$$
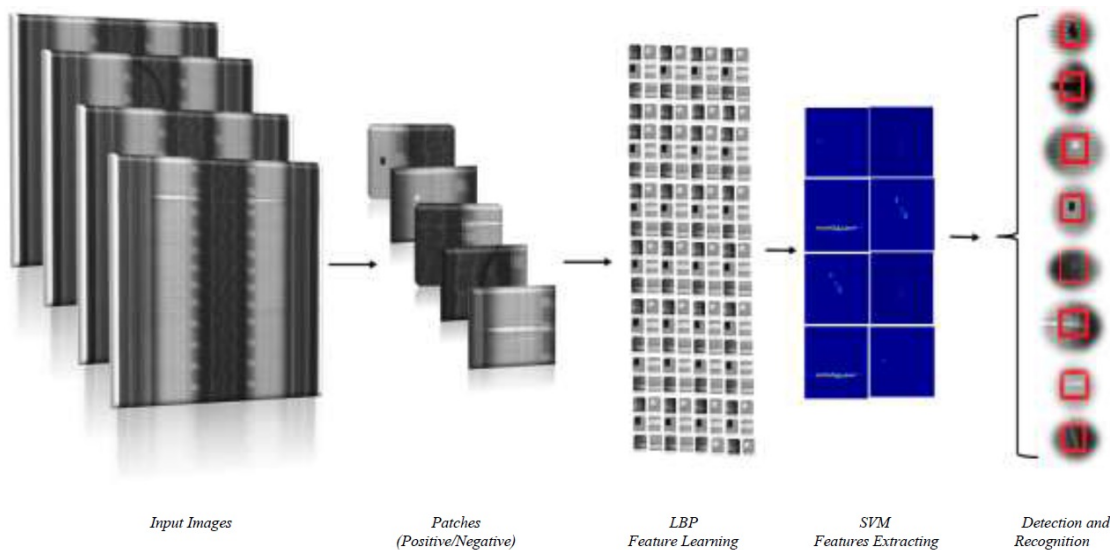

Figure 6: The flowchart of the proposed method

Table 1: Investigation of alignment between research variables

	METHOD	TP	TN	FP	FN	Pr	Re	Acc
0	**Ideal**	2900	100	0	0	1.00	1.00	**100**
1	**KNN-3**	2500	70	277	153	0.900	0.942	**85.66**
2	**KNN-5**	2614	76	206	104	0.926	0.961	**89.63**
3	**Random Forest**	2660	90	183	67	0.935	0.975	**91.56**
4	**SVM-RBF**	2794	96	64	46	0.977	0.983	**96.23**
5	**SVM-Linear**	2843	97	49	11	0.983	0.996	**98.00**

In this equation, N_{cc} is the number of windows that belongs to normal points of the image already recognized by the algorithm as 'non-defect', and N_{dd} is the number of defective windows

already detected as 'defective' by the algorithm. Also, N_{total} is the total number of windows created on the images.

In Table 2, the detection rate that is presented for all types of textural defects in tire images is calculated. In calculating the detection rate in Table 2, it is important that the defective pattern generated by this method is divided into windows with 10×10 dimensions and the window with at least one defective pixel has been considered as a defective window. Therefore, the size of the image is 500×600, and the total number of windows created on the image will be $N_{\text{total}} = 3000$.

It should be noted that in the results obtained in Table 2, an LBP descriptor with a 10×10 window and a linear SVM classifier have been used.

Table 2: Detection rate of the proposed method for different types of defects

Defect type	BFB	SFB	SB	CD	BS	SFC	SBC	SCB
Detection Ratio	98	98	96	96	100	98	94	96

5.2. Classifications of Defects

In this section, the results of the classification for defective regions are given. After diagnosing the stage of defective regions in the previous section, each of these regions is classified into one of eight different types of defects. The defect classification algorithm is described in Section 3. In Fig. 7, a confusion matrix resulting from applying the algorithm is presented to classify the defects. Regarding the confusion matrix, it can be said that the algorithm has no error in the classification of the splice defect. That is due to the structural and situational features for these defects in the images.

Due to the presence of noise and different light conditions, the bubble defect and the foreign object have almost an identical structure.

Therefore, in some cases, the algorithm is wrong in classifying these two categories.

	BFB	SFB	SB	CD	BS	SFC	SBC	SCB
BFB	98	0	2	0	0	0	0	0
SFB	0	98	0	1	0	0	1	0
SB	4	0	96	0	0	0	0	0
CD	0	1	0	96	0	0	3	0
BS	0	0	0	0	100	0	0	0
SFC	0	0	0	0	2	98	0	0
SBC	0	0	0	2	0	0	94	4
SCB	0	0	0	0	0	0	4	96

Figure 7: The confusion matrix of the proposed method for the classification of all tire defects

Also, due to the similarity of the two defects including cord through and over-bending there is also a partial error in classification. According to this Confusion matrix, the accuracy rate of the algorithm in classifying all kinds of defects has been obtained to be 97%.
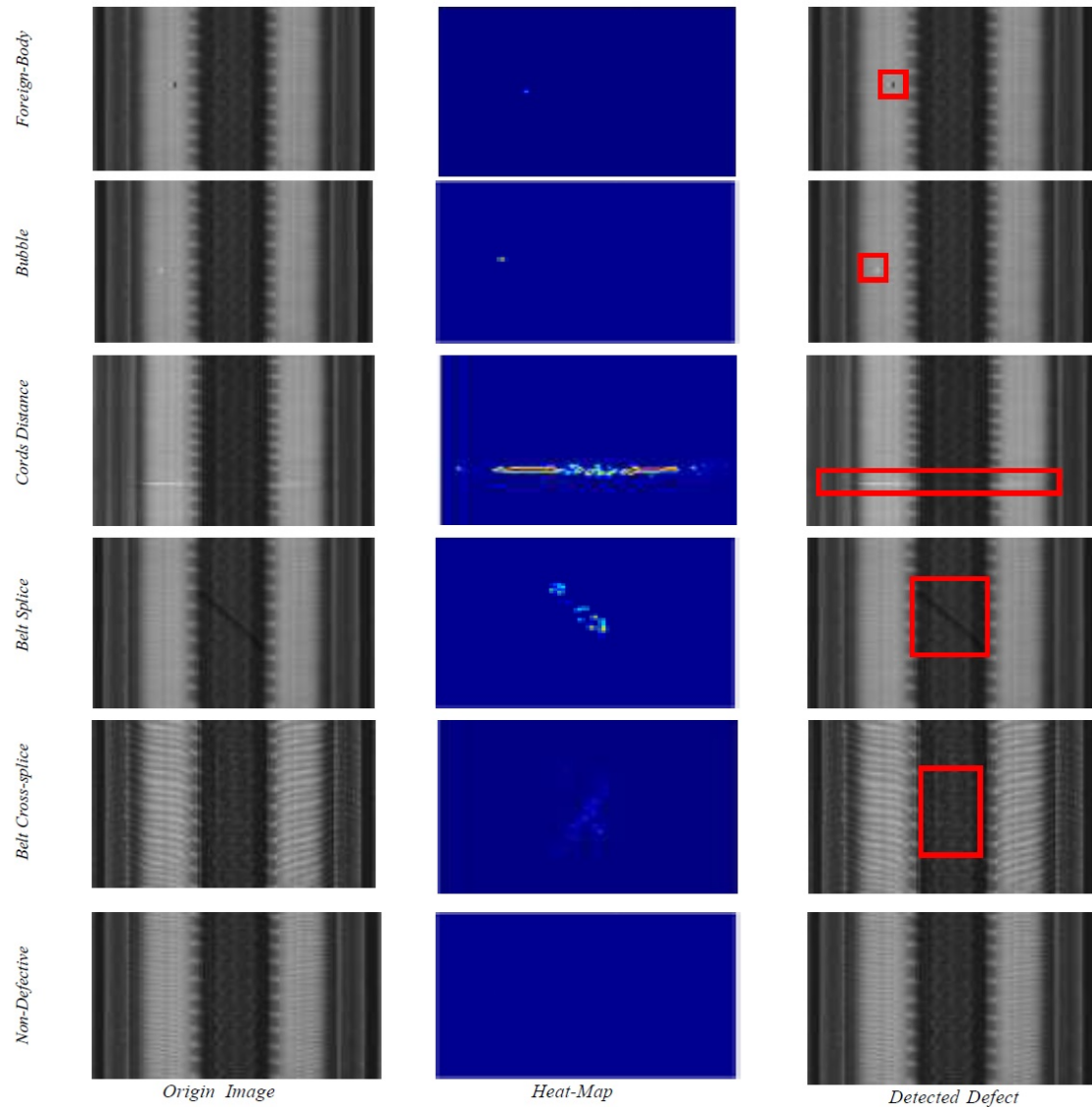
Figure 8: Examples of the implementation of detection and classification algorithm for tire defects.

In Fig. 8, examples of the algorithm output on the defective images have been shown, in which the algorithm has perfectly extracted the defect region and classified its type.

It should be noted that in the course of using this strategy to the problem, other features such as the Histogram of Oriented Gradient (HOG), the second order HOG, and the Gray Level Co-accuracy Matrix (GLCM) were also used to evaluate the accuracy of the system, in which the LBP descriptor achieved a high accuracy. In Fig. 9, the accuracy rate obtained from implementing the algorithm with a combination of different features has been shown.

5.3. Performance of Deep Classifier

In order to analyze the performance of CNN (Convolutional Neural Network) model as a classifier on the proposed pipeline we conducted results using Alex net structure. To do so, we only modify the Alex net structure with changing its input size equal to our extracted patch sizes. Then we trained the model as a binary classification scheme using accuracy metric. The model trained on the patch dataset for 200 epochs. Fig. 10 shows the model convergence through the learning process on this data set. Based on Fig. 10, it is obvious that the model effectively updates its weights and reaches

to its optimal state around 100 epochs; we provided Fig. 11. Fig. 11 shows the effect of increasing the number of epochs on loss decreases. It is manifest that the model decreases the loss in both train and validation set with increasing number of epochs, hence, it illustrates that the model trained well on this data set. In our experimental results, the performance of the proposed pipeline increased approximately 0.3 when we used the deep model as a classifier, thus demonstrating that the deep model has high capability in learning complex patterns.
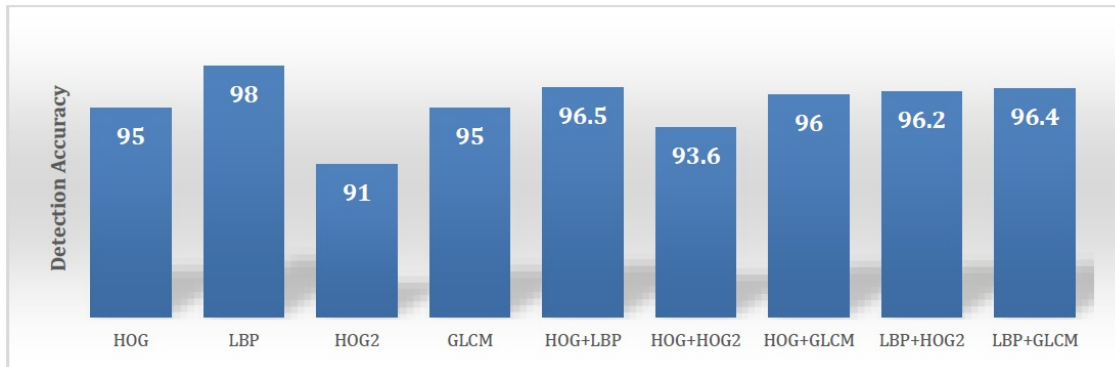

Figure 9: The effect of combining features to enhance the accuracy of the system in identifying defect location
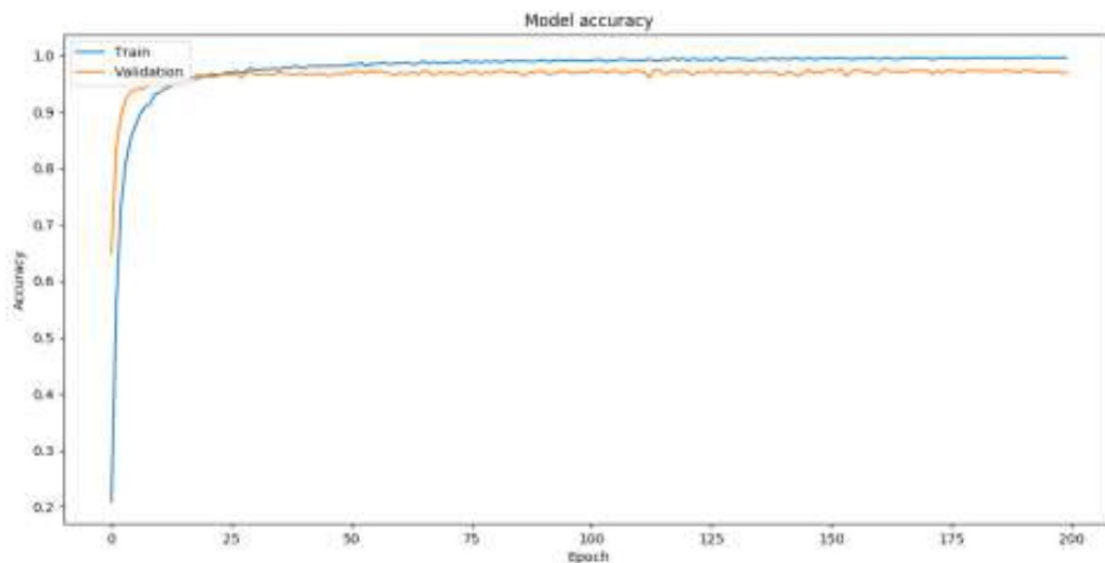

Figure 10: Model convergence rate through the learning process on patch dataset

6. Conclusion

In this paper, a strategy based on image analysis and learning processing was proposed using an entropy filter and an LBP. The proposed strategy, based on the entropy filter analysis, identifies the candidate regions in the image and extracts the local description. Then, the location of the defect and its type are identified with the help of the classification and structural analysis. The tire dataset was collected from Dena Tire and Rubber Manufacturing Company in Iran in order to analyze the strategy. The training and inspection sections were recognized and described in the Dataset section. In the results section, we showed that the best performance was obtained by the LBP descriptor and
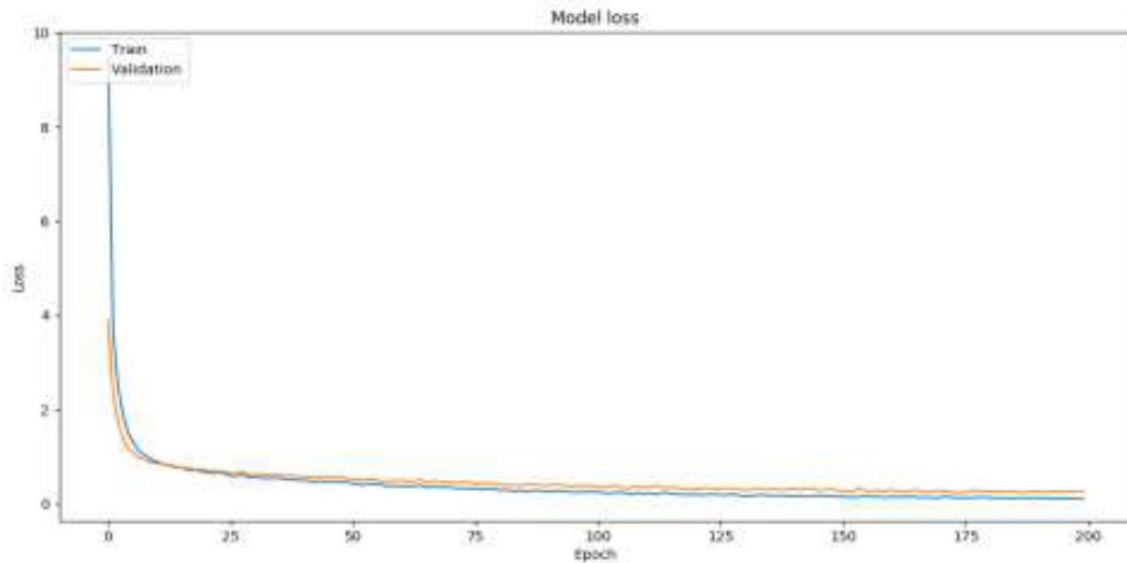
Figure 11: Loss decrease with increasing number of learning epochs

the linear SVM classifier with 98% accuracy (Radical=0.996 and Precision=0.983). Also, according to the results obtained, the LBP that is a hand-crafter descriptor, showed that it was sensitive to local texture and could well describe texture information, which is appropriate for tire defect in X-ray images. Moreover, the effect of the combination of different features and the use of different classification are described in detail. In order to analyze the performance, used the deep model as a classifier that has high capability so in the future, we plan to extract a stronger description of the image region by generalizing this method and presenting a deep learning model so that the algorithm can detect any kind of heterogeneity in similar applications, including all factory produced parts in various companies.

Declarations

Conflict of interest The authors declare that they have no conflict of interest. The manuscript was written through contributions of all authors. All authors have given approval to the final version of the manuscript.

Ethical approval This article does not contain any studies with human participants or animals performed by any of the authors.

References

[1] X. Bai, Y. Fang, W. Lin, L. Wang and B.F. Ju, *Saliency-based defect detection in industrial images by using phase spectrum*, IEEE Trans. Ind. Inf. 10(4) (2014) 2135–2145.

[2] L. Bissi, G. Baruffa, P. Placidi, E. Ricci, A. Scorzoni and P. Valigi, *Automated defect detection in uniform and structured fabrics using Gabor filters and PCA*, J. Visual Commun. Image Represent. 24(7) (2013) 838–845.

[3] X. Chang, C. Gu, J. Liang and X. Xu, *Fabric defect detection based on pattern template correction*, Math. Prob. Engin. 2018 (2018).

[4] C.H. Chien, Y.D. Wu, Y.C. Chen, C.C. Hsieh, T. Chen, Y.T. Chiou, M.L. Tsai, C.T. Wang, S.L. Lin and W.F. Chen, *Quantitative detection of internal defects in automotive tires by an interferographic technique*, Res. Nondest. Eva. 18(3) (2007) 163–177.

[5] X. Cui, Y. Liu, Y. Zhang and C. Wang, *Tire defects classification with multi-contrast convolutional neural networks*, Int. J. Pattern Recogn. Artificial Intell. 32(4) (2018) 1850011.

[6] U. Farooq, T. King, P.H. Gaskell and N. Kapur, *Machine vision using image data feedback for fault detection in complex deformable webs*, Trans. Institute Measur. Control 26(2) (2004) 119–137.

[7] X.F. Feng, *X-Ray Tire Defects Automatic Detection System*, Dissertation, University of Tianjin, 2008.

[8] H. Feng, Z. Jiang, F. Xie, P. Yang, J. Shi and L. Chen, *Automatic fastener classification and defect detection in vision-based railway inspection systems*, IEEE Trans. Instrument. Measur. 63(4) (2013) 877–888.

[9] Q. Guo, C. Zhang, H. Liu and X. Zhang, *Defect detection in tire X-ray images using weighted texture dissimilarity*, J. Sensors 2016 (2016).

[10] Y. Han and P. Shi, *An adaptive level-selecting wavelet transform for texture defect detection*, Image Vision Comput. 25(8) (2007) 1239–1248.

[11] Y.Y. Hung and R.M. Grant, *Shearography: A new optical method for nondestructive evaluation of tires*, Rubber Chem. Technol. 54(5) (1981) 1042–1050.

[12] A. Kumar, *Computer-vision-based fabric defect detection: A survey*, IEEE Transactions on Industrial Electronics, 55(1) (2008) 348–363.

[13] C.F. Kuo and T.L. Su, *Gray relational analysis for recognizing fabric defects*, Textile Res. J. 73(5) (2003) 461–465.

[14] V. Lashkia, *Defect detection in X-ray images using fuzzy reasoning*, Image Vision Comput. 19(5) (2001) 261–269.

[15] Y. Lee and J. Lee, *Accurate automatic defect detection method using quadtree decomposition on SEM images*, IEEE Trans. Semiconductor Manufact. 27(2) (2014) 223–231.

[16] F.Y. Li, *The study of an improved fuzzy edge detection algorithm in radial tire quality detection*, Adv. Mater. Rese. Trans Tech. Publications Ltd, 317 (2011) 968–971.

[17] X. Li, S.K. Tso, X.P. Guan and Q. Huang, *Improving automatic detection of defects in castings by applying wavelet technique*, IEEE Trans. Ind. Electron. 53(6) (2006) 1927–1934.

[18] H. Liu, W. Zhou, Q. Kuang, L. Cao and B. Gao, *Defect detection of IC wafer based on spectral subtraction*, IEEE Trans. Semiconductor Manufact. 23(1) (2010) 141–147.

[19] K.L. Mak and P. Peng, *An automated inspection system for textile fabrics based on Gabor filters*, Robotics Comput.-Integ. Manufact. 24(3) (2008)359–369.

[20] D. Mery and C. Arteta, *Automatic defect recognition in x-ray testing using computer vision*, IEEE Winter Conf. Appl. Comput. Vision (WACV) IEEE, 2017, pp. 1026–1035.

[21] H.Y. Ngan and G.K. Pang, *Regularity analysis for patterned texture inspection*, IEEE Trans. Automation Sci. Engin. 6(1) (2008) 131–144.

[22] H.Y. Ngan, G.K. Pang and N.H. Yung, *Performance evaluation for motif-based patterned texture defect detection*, IEEE Trans. Automation Sci. Engin. 7(1) (2008) 58–72.

[23] H.Y. Ngan, G.K. Pang and N.H. Yung, *Automated fabric defect detection–A review*, Image Vision Comput. 29(7) (2011) 442–458.

[24] J.H. Oh, W.S. Kim, C.H. Han and K.H. Park, *Defect detection of TFT-LCD image using adapted contrast sensitivity function and wavelet transform*, IEICE Trans. Electron. 90(11) (2007) 2131–2135.

[25] T. Ojala, M. Pietikainen and T. Maenpaa, *Multiresolution gray-scale and rotation invariant texture classification with local binary patterns*, IEEE Trans. Pattern Anal. Machine Intell. 24(7) (2002) 971–987.

[26] P.A. Prabha, M. Bharathwaj, K. Dinesh and G.H. Prashath, *Defect detection of industrial products using image segmentation and saliency*, J. Phys. 1916(1) (2021) 012165.

[27] Z. Ren, F. Fang, N. Yan and Y. Wu, *State of the art in defect detection based on machine vision*, Int. J. Precision Engin. Manufacturing-Green Technol. 2021 (2021) 1–31.

[28] Y. Sun, P. Bai, H.Y. Sun and P. Zhou, *Real-time automatic detection of weld defects in steel pipe*, Ndt & E Int. 38(7) (2005) 522–528.

[29] F. Tajeripour, E. Kabir and A. Sheikhi, *Fabric defect detection using modified local binary patterns*, EURASIP J. Adv. Signal Process. 2008 (2007) 1–12.

[30] D.M. Tsai and C.H. Chiang, *Automatic band selection for wavelet reconstruction in the application of defect detection*, Image Vision Comput. 21(5) (2003) 413–431.

[31] D.M. Tsai and T.Y. Huang, *Automated surface inspection for statistical textures*, Image Vision Comput. 21(4) (2003) 307–323.

[32] G. Wang and T.W. Liao, *Automatic identification of different types of welding defects in radiographic images*, Ndt & E Int. 35(8) (2002) 519–528.

[33] M. Win, A.R. Bushroa, M.A. Hassan, N.M. Hilman and A. Ide-Ektessabi, *A contrast adjustment thresholding method for surface defect detection based on mesoscopy*, IEEE Trans. Indust. Inf. 11(3) (2015) 642–649.

[34] Z. Wu, J. Lin and W. Liu, *Joint inspection in X-ray♯ 0 belt tire based on periodic texture*, Multimedia Tools Appl. 78(7) (2019) 9299–9310.

[35] Y. Xiang, C. Zhang and Q. Guo, *A dictionary-based method for tire defect detection*, IEEE Int. Conf. Inf.

Automation (ICIA) IEEE, 2014, pp. 519–523.

[36] L. Xu and Q. Huang, *Modeling the interactions among neighboring nanostructures for local feature characterization and defect detection*, IEEE Trans. Automation Sci. Engin. 9(4) (2012) 745–754.

[37] L. Xu and Q. Huang, *EM estimation of nanostructure interactions with incomplete feature measurement and its tailored space filling designs*, IEEE Trans. Automation Sci. Engin. 10(3) (2013) 579–587.

[38] Z. Yan, L. Tao and L. Qing-Ling, *Detection of foreign bodies and bubble defects in tire radiography images based on total variation and edge detection*, Chinese Phys. Lett. 30(8) (2013) 084205.

[39] Y. Zhang, D. Lefebvre and Q. Li, *Automatic detection of defects in tire radiographic images*, IEEE Trans. Automation Sci. Engin. 14(3) (2015) 1378–1386.

[40] Y. Zhang, T. Li and Q. Li, *Defect detection for tire laser shearography image using curvelet transform based edge detector*, Optics Laser Technol. 47 (2013) 64–71.

[41] Y. Zhu, W.Y. Liu, F.C. Liu and J.J. Wang, *Inspection of air bubble defect in tires by digital holography*, Opt. Prec. Eng. 17 (2009) 1099–1104.